

Cite this: *J. Mater. Chem. C*,  
2026, 14, 4353

# Singlet–triplet gaps for evaluating thermally activated delayed fluorescence: which one is the (b) $E_{ST}$ ?

Ali Shuaib,<sup>a</sup> Lubna Salah,<sup>b,c</sup> Antonio Prlj,<sup>d</sup> Narendran Rajendran,<sup>b</sup>  
Marc K. Etherington,<sup>e</sup> Ahmed Abdel Nazeer,<sup>f</sup> Carlito S. Ponseca Jr,<sup>g</sup>  
Andrew P. Monkman,<sup>h</sup> Andrew Danos<sup>\*,h,i</sup> and Saad Makhseed<sup>\*,b</sup>

The singlet–triplet energy gap ( $\Delta E_{ST}$ ) serves as a central screening parameter for new thermally activated delayed fluorescence (TADF) materials, and is a valuable indicator of eventual OLED performance. Surprisingly though, various measurement methodologies and reporting standards for  $\Delta E_{ST}$  persist across the research community. The resulting variability undermines direct comparisons of material properties across reported works, obfuscating structure–property relationships that would otherwise guide synthetic efforts and computational validation. Here we employ **4CzPyz** and **4tCzPyz** as model systems, and correlate their different possible  $\Delta E_{ST}$  values with their reverse intersystem crossing (rISC) kinetics in films of common and device-relevant hosts. By comparing  $\Delta E_{ST}$  values with emission decay kinetics and device roll-off performance for these two materials, we propose that the steady-state room-temperature photoluminescence onset should be used to determine  $E(S_1)$ , in preference to either steady-state low-temperature or time-resolved singlet emission. Ultimately though, even this should only be taken as an indicator, as device performance is not always reliably predicted by comparing optically derived  $\Delta E_{ST}$  gaps.

Received 16th October 2025,  
Accepted 12th January 2026

DOI: 10.1039/d5tc03735b

rsc.li/materials-c

## 1. Introduction

Thermally activated delayed fluorescence (TADF) has transformed organic light-emitting diode (OLED) technology by enabling complete harvesting of electrically generated excitons without requiring precious heavy-metal phosphors.<sup>1–4</sup> This breakthrough emerges from the thermal upconversion of non-emissive triplet states to

emissive singlets through reverse intersystem crossing (rISC), avoiding the 25% efficiency limit imposed by spin statistics in conventional fluorescent materials.<sup>5–7</sup> The efficiency of this process depends exponentially on the singlet–triplet energy gap ( $\Delta E_{ST}$ ), establishing its accurate determination and comparison as a cornerstone of TADF material development.<sup>8–10</sup>

Despite this central importance,  $\Delta E_{ST}$  determination using different common spectroscopic methods sometimes yields dramatically conflicting values for identical materials, with variations exceeding 250 meV.<sup>11–13</sup> This inconsistency represents more than an experimental inconvenience; often silently, it undermines the fundamental premise of rational TADF design and precludes direct comparison of experimental results across different research groups.<sup>14–16</sup> Even in this context recent works attempt to directly minimize  $\Delta E_{ST}$ ,<sup>17</sup> carefully quantify its different values,<sup>18</sup> or examine its inversion all towards more efficient OLED operation.<sup>19</sup> It therefore remains timely to consider what really is the most appropriate way to measure and report this seemingly simple spectroscopic parameter.

The different potential reporting methods for  $\Delta E_{ST}$  primarily arise from the temporal complexity of TADF photophysics, itself a consequence of the conformational flexibility of donor–acceptor architectures (Fig. 1).<sup>20</sup> Following photoexcitation,

<sup>a</sup> Biomedical Engineering Unit, Department of Physiology, Faculty of Medicine, Kuwait University, P.O. Box 24923, Safat-13110, Kuwait.  
E-mail: ali.shuaib@ku.edu.kw

<sup>b</sup> Department of Chemistry, Faculty of Science, Kuwait University, P.O. Box 5969, Safat-13060, Kuwait. E-mail: saad.makhseed@ku.edu.kw

<sup>c</sup> Faculty of Chemistry, Silesian University of Technology, Strzody 9, 44-100, Gliwice, Poland

<sup>d</sup> Division of Physical Chemistry, Ruđer Bošković Institute, Bijenička cesta 54, 10000, Zagreb, Croatia

<sup>e</sup> School of Engineering, Physics and Mathematics, Northumbria University, Ellison Place, Newcastle upon Tyne NE1 8ST, UK

<sup>f</sup> Nanotechnology Applications Program, Energy and Building Research Center, Kuwait Institute for Scientific Research, P.O. Box 24885, Safat-13109, Kuwait

<sup>g</sup> Department of Mathematics and Natural Sciences, Gulf University for Science and Technology, Hawally, Kuwait

<sup>h</sup> Department of Physics, Durham University, South Road, Durham DH1 3LE, UK

<sup>i</sup> School of Physical and Chemical Sciences, Queen Mary University of London, London E1 4NS, UK. E-mail: a.danos@qmul.ac.uk

† These authors contributed equally to this work.



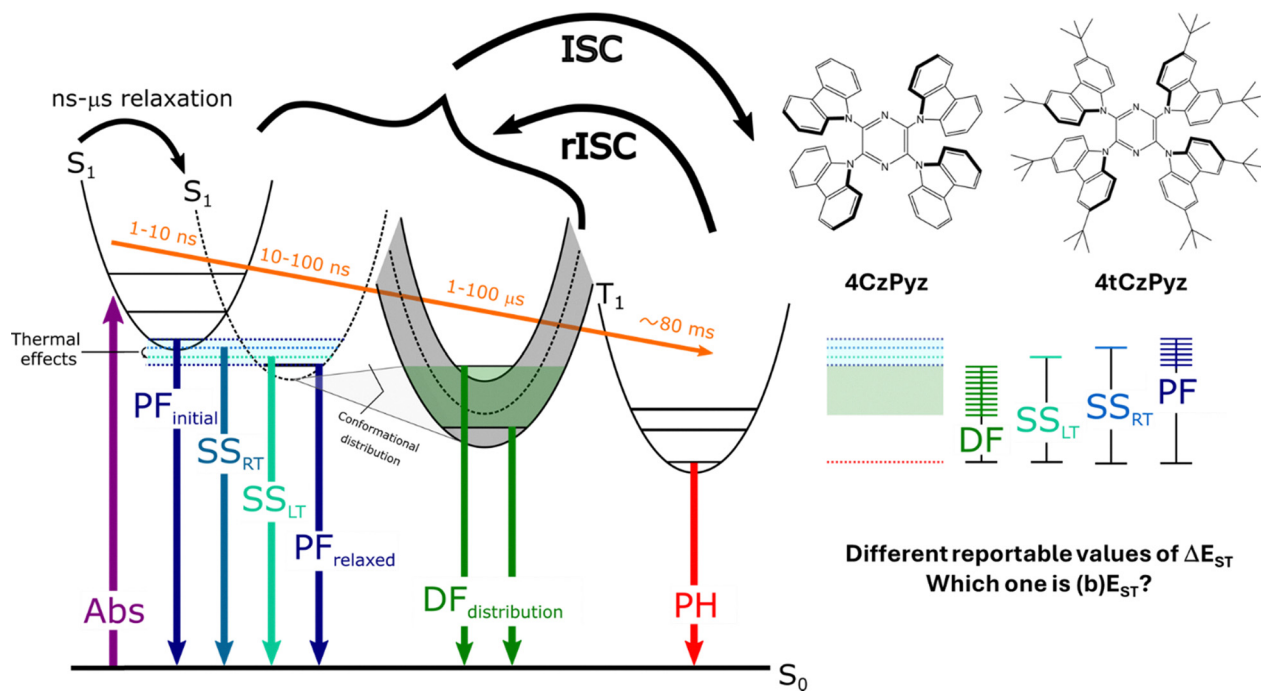


**Fig. 1** Temporal evolution of excited states in TADF materials (left), and the resulting range of reportable  $\Delta E_{ST}$  values (right). Following photoexcitation, molecules undergo conformational relaxation during prompt fluorescence (PF, ns regime) and delayed fluorescence (DF,  $\mu$ s to ms regime) proceeding via reverse intersystem crossing (rISC). Steady-state methods (room-temperature,  $SS_{RT}$ ; and low-temperature,  $SS_{LT}$ ) provide single ensemble-averaged values. Time-resolved approaches (PF, DF) yield variable results depending on the selected temporal window. Phosphorescence (PH) measurements determine triplet state energies, but are often only accessible at low temperatures. The shaded sections (right) depict the ranges of possible singlet energies that could be selected from different measurements, thus illustrating the range of reportable  $\Delta E_{ST}$  values (black/coloured bars) relative to the same triplet energy (red dotted line). Molecular structures of **4CzPz** and **4tCzPz** are shown in the upper right.

molecules undergo conformational relaxation during prompt fluorescence (PF, nanosecond timescale), followed by intersystem crossing and thermal activation enabling rISC and delayed fluorescence (DF, microsecond to millisecond timescale).<sup>21–23</sup> Each of the commonly used reporting methods for  $\Delta E_{ST}$  (discussed below) samples different temporal windows of this evolution, potentially capturing distinct conformational subsets with different emission energies.<sup>24–27</sup>

In principle the difference in energy between the  $S_1$  and  $T_1$  states simply defines  $\Delta E_{ST} = E(S_1) - E(T_1)$ .  $E(T_1)$  can be estimated from the high-energy onset of the phosphorescence (PH) spectrum acquired using low-temperatures and long acquisition delays following pulsed excitation to eliminate contribution from both PF (time-resolved) and DF (temperature suppressed). In cases where the phosphorescence arises from locally excited (LE) states with strong vibronic structured emission, the shortest wavelength peak of the spectrum is also occasionally used. For TADF materials with mixed charge transfer (CT) and LE excited state character such a peak is not always readily identifiable for  $T_1$  assignment, and the onset is often more appropriate.

While estimation of  $E(T_1)$  is usually relatively straightforward, the situation for  $E(S_1)$  is surprisingly fraught. Steady-state room-temperature ( $SS_{RT}$ ) fluorescence emission is the most convenient and most frequently used to estimate the  $E(S_1)$  value, but this neglects any changes in molecular

conformation that may impact  $E(T_1)$  (necessarily measured at low-temperature). Proponents of using steady-state low-temperature measurements ( $SS_{LT}$ ) for  $E(S_1)$  can rightly claim that this version of  $\Delta E_{ST}$  at least controls for any temperature-associated changes in molecular geometry, however it is the room-temperature value of  $E(S_1)$  and associated molecular conformers that are actually relevant to ambient operation of OLED devices. Steady-state measurements themselves present a single onset value as the intensity-weighted ensemble average of different conformers in a film sample, in contrast to time-resolved values that can change significantly depending on the delay time chosen as molecular conformations relax following excitation. The desirable removal of user choice in these steady-state values is therefore counterbalanced by the consideration that it is the molecular conformers emitting in the DF regime that are actually responsible for rISC in TADF devices. Hence of these four common variants of  $\Delta E_{ST}$  ( $SS_{RT}$ -PH,  $SS_{LT}$ -PH, PF-PH, and DF-PH), none stands out as a clear ‘best’ choice for predicting rISC and OLED performance.

Here we examine this challenge through systematic comparison of **4CzPz**<sup>28,29</sup> and **4tCzPz**<sup>30</sup> as model systems, exhibiting similar spectra but different  $\Delta E_{ST}$  and rISC kinetics. We take the view that the usefulness of any version of  $\Delta E_{ST}$  is in its ability to predict trends in rISC and DF lifetimes, and thus also OLED performance. Hence by comparing these kinetic and spectroscopic properties, we come to the conclusion that the



steady-state room-temperature  $E(S_1)$  is likely the best to use, but ultimately confirm that none of the  $\Delta E_{ST}$  variants give anything more than an indication of device performance.

## 2. Results and discussion

To systematically evaluate these measurement approaches, we selected **4CzPyz**<sup>28,29</sup> and **4tCzPyz**<sup>30</sup> (shown in Fig. 1) as model systems. These compounds differ only by *tert*-butyl substitution on the carbazole donors, yet exhibit different rISC kinetics despite having similar excited states. We examined both compounds across three strategically chosen host environments: Zeonex (apolar), DPEPO (polar), and PPT (for which device results are already reported<sup>29,30</sup>). Although the core utility of  $\Delta E_{ST}$  measurements is usually to indicate these kinetics and device performance properties ahead of time, this full investigation instead allows us to confirm how faithfully the different versions of  $\Delta E_{ST}$  make these predictions. The chemical similarity of these two emitters allows us to also confidently attribute changes in kinetics to changes in  $\Delta E_{ST}$ , as both are expected to have similar spin-orbit coupling (D–A structure with no heavy atoms) and vibronic coupling between excited states (discussed below).<sup>21,22</sup>

Fig. 2 presents comprehensive steady-state characterization of both emitters in the varying host environments, at both room-temperature ( $SS_{RT}$ ) and 80 K ( $SS_{LT}$ ). Both compounds exhibit broad emission bands characteristic of charge-transfer singlet states, with dramatic host-dependent spectral shifts reflecting their sensitivity to host environment. The phosphorescence

spectra reveal very similar  $E(T_1)$  across the series, likely arising from the shared pyrazine core. For all measurements except **4CzPyz** in PPT, the low-temperature spectra red-shift relative to room-temperature emission, although only by  $\sim 0.03$  eV.

Fig. 3 and 4 illustrate the continuous evolution of the singlet emission throughout both PF and DF regimes. These changes in onset demonstrate the challenge of selecting “representative” time points for  $E(S_1)$ , and therefore also  $\Delta E_{ST}$  determination. During PF (0.8–50 ns), systematic red-shifts reflect conformational relaxation from initially excited Franck–Condon geometries, toward thermally equilibrated structures. The DF regime exhibits even more dramatic spectral migration, with substantial shifts from early microsecond to late millisecond timescales. This pronounced evolution arises from the complex population dynamics in the emitting films, where different conformational subsets exhibit varying spectra and kinetics.<sup>20</sup> The continuous spectral evolution demonstrates that any single temporal snapshot provides an at-best incomplete and potentially misleading representation of the ensemble behavior. It is also unclear which of these subsets is primarily responsible for device performance.

The different onset-derived values for  $\Delta E_{ST}$  (or possible ranges for time-resolved onsets) are presented in Table 1. The same values are also shown graphically in Fig. 5a. Inspecting this figure, we attempt to identify trends in the values of  $\Delta E_{ST}$  when comparing **4CzPyz** and **4tCzPyz** in the same host environment, which correspond to performance predictions that can be later compared to the actual kinetics and device measurements. In Zeonex, **4tCzPyz** is found to have a smaller  $\Delta E_{ST}$  than **4CzPyz** regardless of measurement method, and there is no

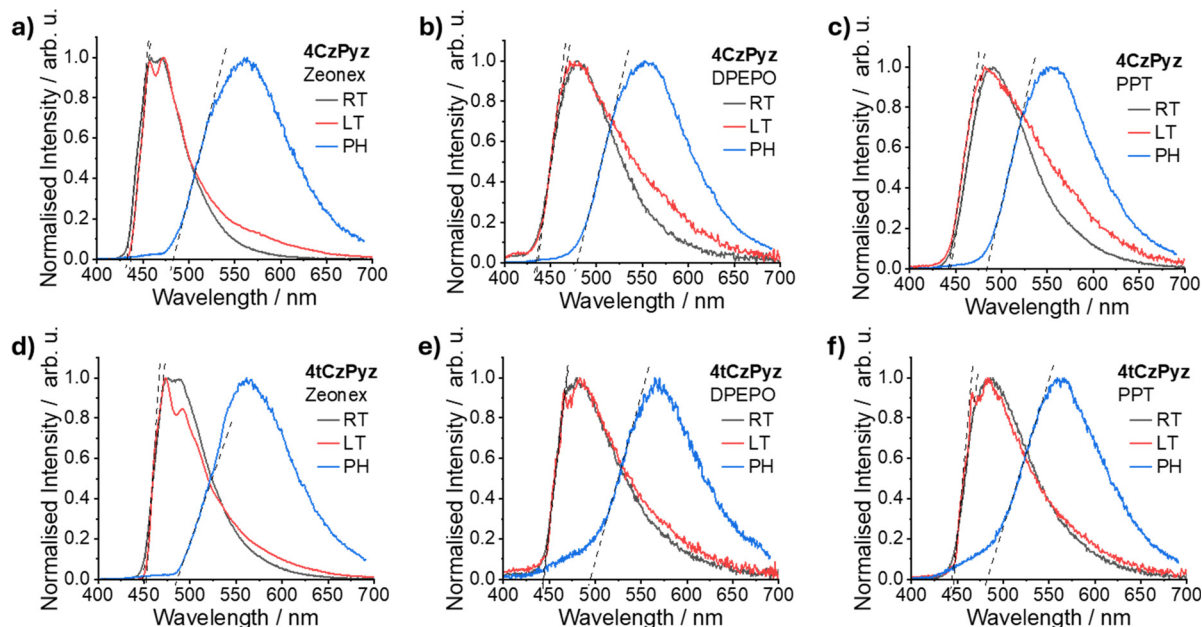


Fig. 2 Steady-state photoluminescence characterization of **4CzPyz** (a)–(c) and **4tCzPyz** (d)–(f) across three host environments (1 wt% Zeonex, 10 wt% DPEPO, and 10 wt% PPT films). Each panel shows room-temperature steady-state emission (RT, black), low-temperature steady-state emission (LT taken at 80 K, red), and 80 K time-resolved phosphorescence spectra (PH taken at 80 ms following pulsed excitation, blue). Black dashed tangent lines indicate the spectral onsets used in determination of individual state energies and hence  $\Delta E_{ST}$ .



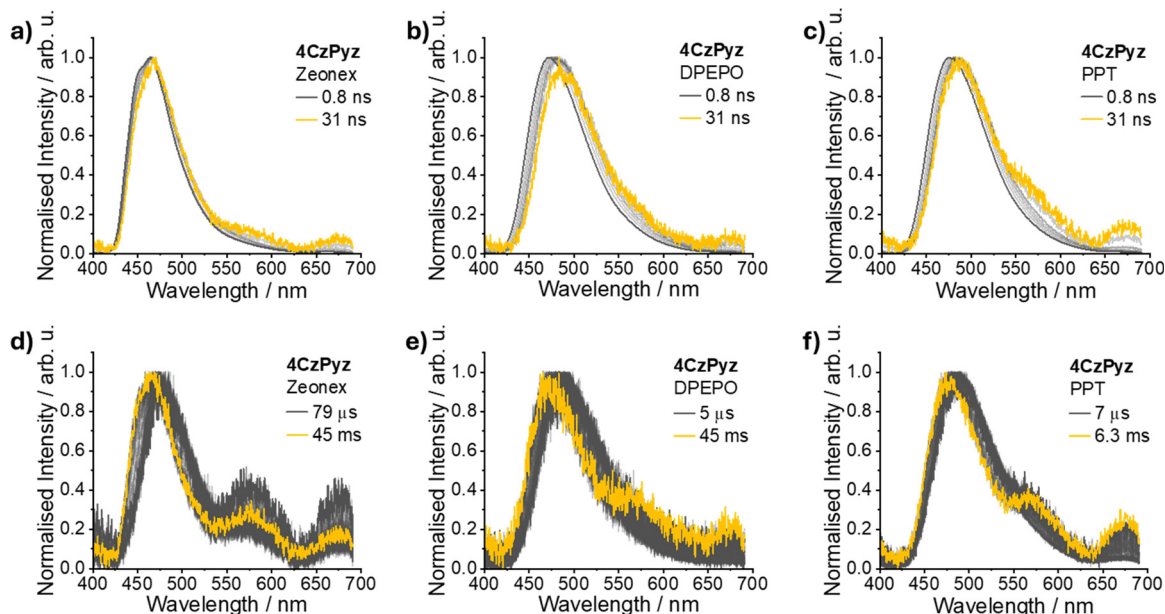


Fig. 3 Time-resolved photoluminescence spectra of **4CzPyz** showing temporal evolution during (a)–(c) prompt fluorescence (PF, 0.8–31 ns) and (d)–(f) delayed fluorescence (DF,  $\mu$ s–ms) regimes across three host environments (1 wt% Zeonex, 10 wt% DPEPO, and 10 wt% PPT films).

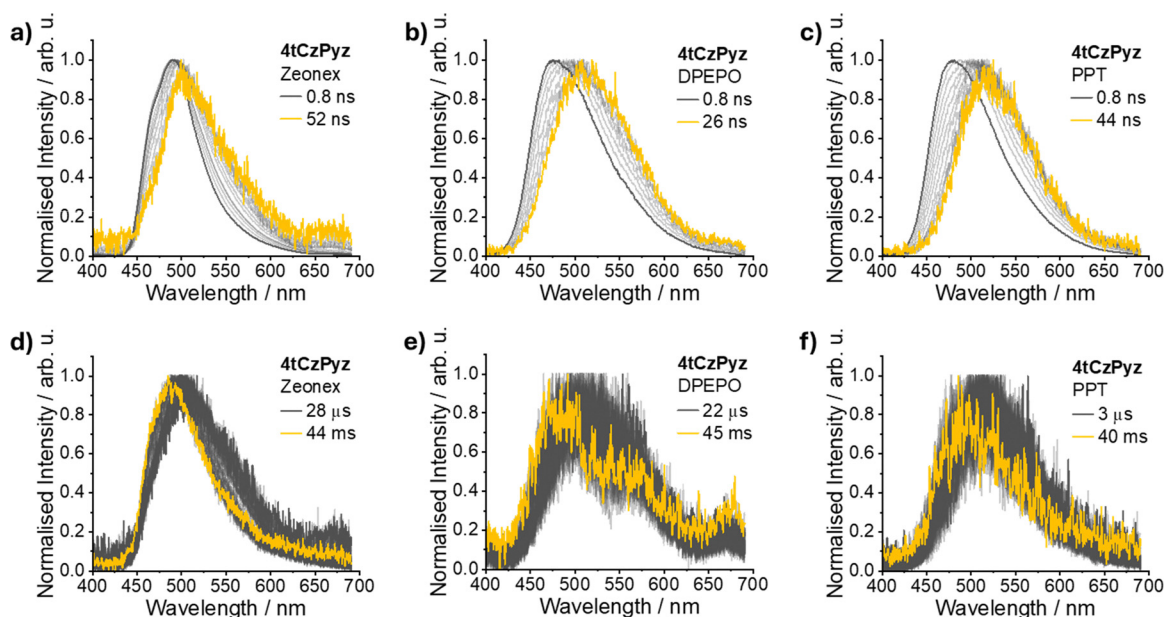


Fig. 4 Time-resolved photoluminescence spectra of **4tCzPyz** showing temporal evolution during (a)–(c) prompt fluorescence (PF, 0.8–52 ns) and (d)–(f) delayed fluorescence (DF,  $\mu$ s–ms) regimes across three host environments (1 wt% Zeonex, 10 wt% DPEPO, and 10 wt% PPT films).

overlap between their respective  $\Delta E_{ST}$  value ranges whether derived from PF or DF onsets. This agrees with theoretical calculations for these two emitters in vacuum using a nuclear ensemble approach<sup>31–33</sup> (NEA, Fig. 5b), sampling across 500 geometries from a harmonic Wigner distribution of the  $T_1$  state at 80 K.

Excited state energies and hence  $\Delta E_{ST}$  values for these geometries were calculated using DFT/TDDFT (see computational details in SI), with the gas-phase calculations most

comparable to the measurements of the dilute and inert Zeonex films. Indeed the lower-energy onsets of the  $\Delta E_{ST}$  histograms appear to reproduce the experimental  $SS_{RT/LT}$   $\Delta E_{ST}$  measurements, at approximately 0.2 and 0.3 eV for **4tCzPyz** and **4CzPyz** respectively. Although the modes of the histograms occur at larger  $\Delta E_{ST}$  values, we propose that it is the molecules with the smallest values that will most strongly contribute to the DF properties. We were also required to restrict our investigation to  $T_1$  geometries and low temperatures in this work in order to



**Table 1** Comparison of singlet–triplet energy gaps ( $\Delta E_{ST}$ , eV) for **4CzPyz** and **4tCzPyz** determined using four different measurement methods: room-temperature steady-state ( $SS_{RT}$ -PH), low-temperature steady-state ( $SS_{LT}$ -PH), prompt fluorescence onset (PF-PH), and delayed fluorescence onset (DF-PH) approaches across 1 wt% Zeonex, 10 wt% DPEPO, and 10 wt% PPT host environments. For PPT, an additional version using previously reported device<sup>29,30</sup> electroluminescence onsets is also provided (EL-PH)

Host	Compound	$SS_{RT}$ - PH	$SS_{LT}$ - PH	PF <sub>max</sub> - PH	PF <sub>min</sub> - PH	DF <sub>max</sub> - PH	DF <sub>min</sub> - PH	EL - PH
Zeonex	4CzPyz	0.30	0.27	0.35	0.33	0.34	0.26	—
	4tCzPyz	0.21	0.19	0.25	0.24	0.26	0.23	—
DPEPO	4CzPyz	0.26	0.25	0.30	0.23	0.30	0.21	—
	4tCzPyz	0.29	0.28	0.39	0.32	0.38	0.28	—
PPT	4CzPyz	0.23	0.24	0.31	0.26	0.30	0.25	0.26
	4tCzPyz	0.22	0.21	0.29	0.13	0.27	0.19	0.22

Note: All  $\Delta E_{ST}$  values calculated using singlet energies from the respective methods and triplet energies from 80 K phosphorescence (PH) onset. PF max/min and DF max/min represent the largest/smallest  $\Delta E_{ST}$  values obtained from different spectra within the respective temporal regimes (See Fig. 3 and 4).

manage computational costs. This combination would most closely correspond to experimental  $\Delta E_{ST}$  measurements derived from DF-PH comparisons of time-resolved measurements taken at low temperature, as DF emission arises initially from rISC in triplet molecular geometries. Experimentally this specific measurement is not accessible though, as at low temperatures the DF itself would be suppressed. Future investigations may allow this computational approach to also simulate and predict changes in  $\Delta E_{ST}$  as derived from measurements across the PF and  $SS_{RT}$ , by considering energies of separate  $S_1$  geometry distributions at elevated temperatures. The impact of host molecules can also be included, although again at considerable computational expense.<sup>34</sup>

Returning to Fig. 5a, for the measurements in DPEPO both steady-state measurements ( $SS_{RT}$  and  $SS_{LT}$ ) lead to smaller  $\Delta E_{ST}$  values for **4CzPyz**, although there is overlap and potential disagreement in predictions between methods depending on which of the time-resolved measurements are selected for comparison. In PPT this overlap is even more severe, although both PF and DF extend across smaller  $\Delta E_{ST}$  values for **4tCzPyz**. **4tCzPyz** in PPT also gives a particularly wide range of PF-derived  $\Delta E_{ST}$  values (visible in Fig. 4c), which may arise from a wider range of microenvironment heterogeneity, or from a wider range of donor–acceptor dihedral angles in the molecules in the film (disorder), that relax gradually upon photoexcitation.<sup>20</sup> Regardless of the cause, it appears that this major shift across the PF has no subsequent impact on the DF kinetics compared to **4CzPyz** (Fig. 6c). Interestingly, for PPT the ordering of the room- and low-temperature steady-state ( $SS_{RT}$  and  $SS_{LT}$ )  $\Delta E_{ST}$  measurements inverts for **4CzPyz**, in contrast to all other measurements.

To critically evaluate the ability of the different versions of  $\Delta E_{ST}$  to predict rISC performance, Fig. 6 shows the time-resolved photoluminescence decays of the same films. RT decay profiles reveal only subtle differences in delayed emission kinetics, as might be predicted from their overall similar  $\Delta E_{ST}$  values. In Zeonex films **4CzPyz** exhibits slightly slower and lower intensity DF compared to **4tCzPyz**, in agreement with the  $\Delta E_{ST}$  of the latter being smaller for all four considered variants and in calculations. In DPEPO the kinetic ordering inverts, with **4CzPyz** showing faster-decaying DF with

comparable intensity. This outcome is predicted by both the  $SS_{RT}$  and  $SS_{LT}$   $\Delta E_{ST}$  values as well as those derived from PF spectra (smaller for **4CzPyz**), however the overlap of DF onset ranges means this prediction cannot also be confidently made for this version of  $\Delta E_{ST}$ .

PPT films yield nearly identical photoluminescence decay profiles, shown in Fig. 6c. This is consistent with  $SS_{RT}$   $\Delta E_{ST}$  values being nearly identical, while the  $SS_{LT}$  variant of  $\Delta E_{ST}$  incorrectly predicts faster decay kinetics for **4tCzPyz** by a similar expected magnitude of difference as seen for DPEPO. Here as well the time-resolved ranges of  $\Delta E_{ST}$  values significantly overlap, such that any predictive power is overshadowed by the choice of specific spectra used. Hence, it appears from the measurements in PPT that the  $SS_{RT}$  variant of  $\Delta E_{ST}$  is the most predictive of the time-resolved kinetics and underpinning rISC. We do not attempt to directly quantify these rISC rates though, as they can similarly strongly depend on the range of decay used to fit prompt and delayed lifetimes.<sup>7</sup>

Before progressing we must consider other possible mechanisms by which the *t*Bu groups in **4tCzPyz** can impact rISC, and hence justify the earlier assertion that the structural similarity of **4CzPyz** and **4tCzPyz** allows the changes in TADF kinetics to be attributed to changes in  $\Delta E_{ST}$ . In the first instance, by increasing the electron-donating strength of the Cz groups the *t*Bu substituents are able to directly impact  $E(S_1)$  and hence modify  $\Delta E_{ST}$ .<sup>35</sup> In addition, *t*Bu groups have been shown to reduce the formation of aggregate states,<sup>36,37</sup> although for the low-concentration films investigated here this is not of primary concern. While *t*Bu groups can also influence the steric environment of donor groups in crowded multi-Cz emitters,<sup>38</sup> we have previously shown that the pyrazine heteroatoms in **4CzPyz**<sup>28</sup> and similar materials<sup>39</sup> significantly alleviate steric congestion near the D–A bond. This environment limits the potential for outwardly-pointing *t*Bu groups to influence the equilibrium D–A dihedral angle, although any such changes will also then reflect in  $\Delta E_{ST}$  itself through changes in the electronic coupling between donor and acceptor units. Separately, any ‘inertial’ effects of the *t*Bu groups reducing vibronic coupling (by dampening the relevant D–A bond torsions) are expected to be small – inertial impacts on rISC were only modest in fluid solutions for previously reported



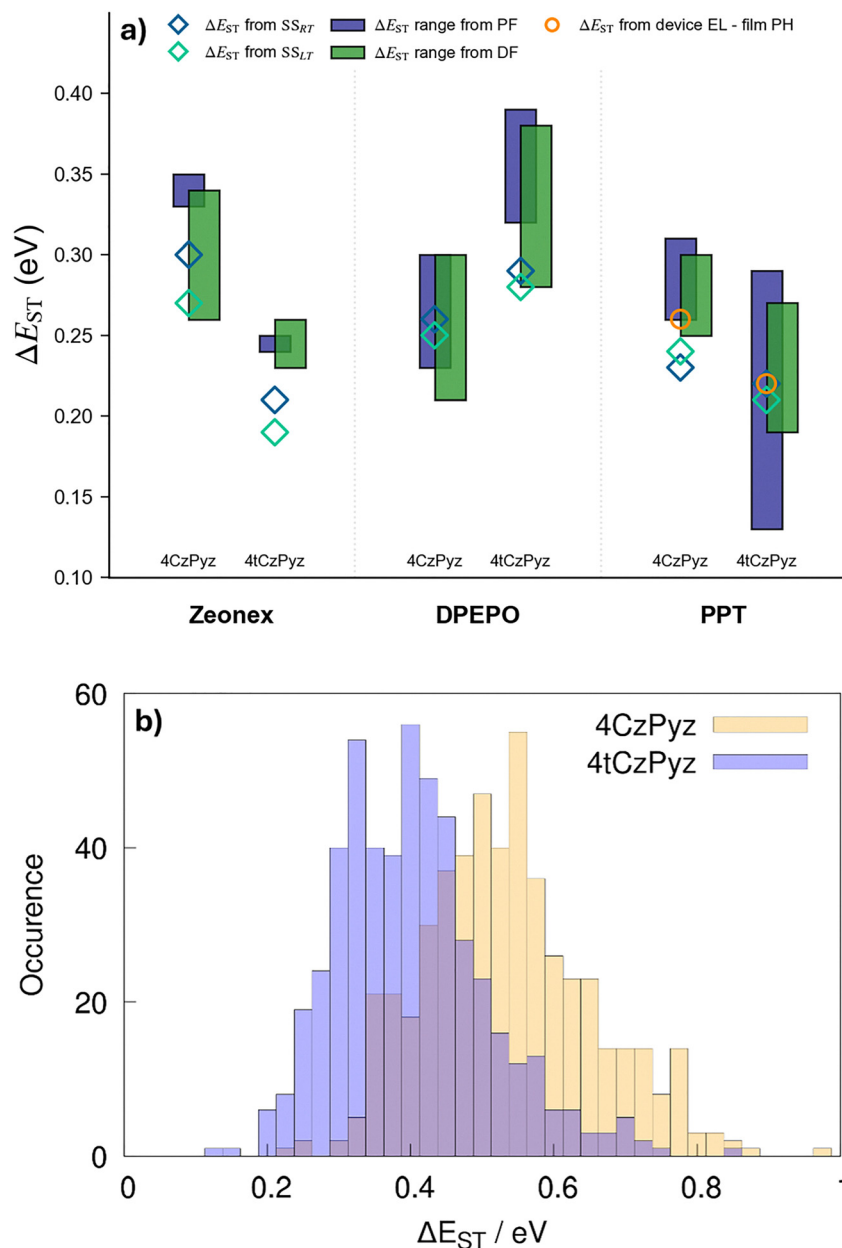


**Fig. 5** (a) Comparison of  $\Delta E_{ST}$  values obtained using different approaches for **4CzPyz** and **4tCzPyz** across three host environments (1 wt% Zeonex, 10 wt% DPEPO, and 10 wt% PPT). Dark blue diamonds indicate  $\Delta E_{ST}$  values from  $SS_{RT}$  onset, while cyan diamonds indicate  $\Delta E_{ST}$  values from  $SS_{LT}$  onsets. Navy bars represent the range of  $\Delta E_{ST}$  values inferable from prompt fluorescence (PF) onset measurements, with green bars showing similar for delayed fluorescence (DF) onsets. Orange circles indicate the  $\Delta E_{ST}$  values derived from the device electroluminescence (EL) onset (PPT film only) ref. 29 and 30. All  $\Delta E_{ST}$  values were calculated using triplet energies derived from 80 K phosphorescence (PH) onsets. (b) Histogram of  $\Delta E_{ST}$  values calculated using DFT/TDDFT across ensembles of molecules in their  $T_1$  geometries at 80 K.

materials featuring much larger and more axially-displaced adamantyl substituents, and only barely discernable in solids films.<sup>40</sup>

From the near identical  $\Delta E_{ST}$  values and near identical emission decays in PPT, we would therefore infer near-identical rISC rates and hence expect near-identical OLED performance from **4CzPyz** and **4tCzPyz**. Indeed, previously reported devices of these emitters in identical stacks with PPT host show very similar  $EQE_{max}$  (Fig. 7a). However, while  $EQE_{max}$  relies on both

rISC and emitter PLQY (reported at 75 and 73% for **4CzPyz** and **4tCzPyz**, respectively in PPT), the roll-off of this EQE is more strongly determined by rISC and shows significant unexpected differences at higher operating brightnesses. Comparing the two devices together, the roll-off for **4tCzPyz** is significantly improved, in contrast to the similar spectroscopic  $\Delta E_{ST}$  and even rISC inferred from comparison of time-resolved emission kinetics. This comparison therefore demonstrates that none of the variants of  $\Delta E_{ST}$  are able to make 'ironclad' predictions of



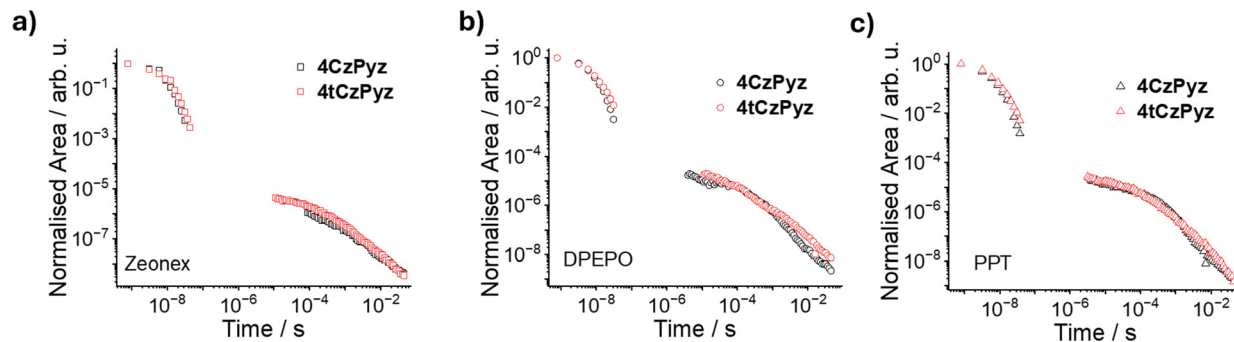


Fig. 6 Room-temperature photoluminescence decay profiles of **4CzPz** and **4tCzPz** in (a) 1 wt% Zeonex, (b) 10 wt% DPEPO, and (c) 10 wt% PPT host environments.

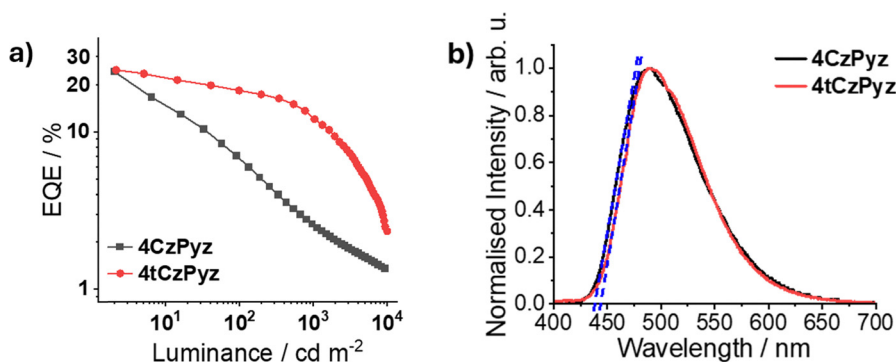


Fig. 7 OLED device performance and electroluminescence characterization. (a) External quantum efficiency (EQE) versus luminance ( $\text{cd m}^{-2}$ ) characteristics for OLED devices. (b) Normalized electroluminescence (EL) spectra of OLED devices based on **4CzPz** and **4tCzPz** at 10 wt % in PPT. Dashed blue tangent lines indicate the spectral onsets used for determining  $\Delta E_{\text{ST}}$  from EL-PH. Device data taken from ref. 29 and 30.

device performance for **4CzPz** and **4tCzPz** specifically, and thus proves by contradiction that similar skepticism should be applied for TADF materials more broadly.

Instead, here  $\Delta E_{\text{ST}}$  taken from the onset of device electroluminescence (EL, Fig. 7b) does correspond with the device roll-off, and is considerably smaller for **4tCzPz** as shown in Fig. 5a and Table 1. It is unclear whether these different device-emission onsets are a result of the EL process, or potentially the evaporated nature of the emissive films. In either case though, requiring device preparation and characterization to enable accurate ‘prediction’ of device performance is of limited strategic value, as the ‘prediction’ made by this version of  $\Delta E_{\text{ST}}$  is itself immediately superseded by the direct device measurements.

While the use of  $\Delta E_{\text{ST}}$  to broadly or qualitatively predict trends in TADF materials (where these values sufficiently differ) is therefore still useful, and our recommended standardization of reporting using  $\text{SS}_{\text{RT}}$  measurements may help support greater meta-analytical insight across the research community, we ultimately demonstrate that the performance of devices is not guaranteed to be predicted by this factor in any of its spectroscopic variants. This work therefore justifies the abandonment of pedantic or over-zealous support of any single reporting method, while weakly favoring  $\text{SS}_{\text{RT}}$

measurements primarily for their convenience and towards a unified approach.

### 3. Conclusion

Through systematic evaluation and comparison to further spectroscopic and optoelectronic characterization, we demonstrate that room-temperature steady-state ( $\text{SS}_{\text{RT}}$ ) measurements provide the most convenient and reliable approach for determining predictive  $\Delta E_{\text{ST}}$ , albeit by only a narrow margin. The more important performance of actual devices is only loosely tied to any version of  $\Delta E_{\text{ST}}$ , and quantitative comparisons are not necessarily insightful especially when the differences are small. While it will benefit the community to adopt a single reporting standard across the research field, the direct benefits of choosing any particular method within a single investigation are limited. Based on experimental convenience and the removal of user choice, we recommend the use of  $\text{SS}_{\text{RT}}$   $E(S_1)$  measurements, but stress that none of these methods can be uncritically relied on to fully predict eventual device performance.

### Conflicts of interest

There are no conflicts to declare.



## Data availability

All relevant data is presented in the main text. Supporting information (SI): general and computational methods, synthetic procedures, and characterization data for **4tCzPyz**. See DOI: <https://doi.org/10.1039/d5tc03735b>.

## Acknowledgements

The authors gratefully acknowledge the Kuwait Foundation for the Advancement of Science (KFAS, grant number CN22-15SC-1583). The authors also thank Kuwait University for providing access to Research Sector Project Units (RSPU) general facilities of the Faculty of Science (GFS; GS 01/01, GS 01/03, GS 01/05, GS 01/08, GS 02/01, GS 02/13, GS 03/01, GS 03/08). We further thank Prof Eli Zysman-Colman for providing access to device data previously published for **4CzPyz** and **4tCzPyz** in PPT.

## References

- H. Uoyama, K. Goushi, K. Shizu, H. Nomura and C. Adachi, Highly Efficient Organic Light-Emitting Diodes from Delayed Fluorescence, *Nature*, 2012, **492**(7428), 234–238, DOI: [10.1038/nature11687](https://doi.org/10.1038/nature11687).
- A. Endo, K. Sato, K. Yoshimura, T. Kai, A. Kawada, H. Miyazaki and C. Adachi, Efficient Up-Conversion of Triplet Excitons into a Singlet State and Its Application for Organic Light Emitting Diodes, *Appl. Phys. Lett.*, 2011, **98**(8), 083302, DOI: [10.1063/1.3558906](https://doi.org/10.1063/1.3558906).
- Z. Yang, Z. Mao, Z. Xie, Y. Zhang, S. Liu, J. Zhao, J. Xu, Z. Chi and M. P. Aldred, Recent Advances in Organic Thermally Activated Delayed Fluorescence Materials, *Chem. Soc. Rev.*, 2017, **46**(3), 915–1016, DOI: [10.1039/C6CS00368K](https://doi.org/10.1039/C6CS00368K).
- J. M. Dos Santos, D. Hall, B. Basumatary, M. Bryden, D. Chen, P. Choudhary, T. Comerford, E. Crovini, A. Danos, J. De, S. Diesing, M. Fatahi, M. Griffin, A. K. Gupta, H. Hafeez, L. Hämmerling, E. Hanover, J. Haug, T. Heil, D. Karthik, S. Kumar, O. Lee, H. Li, F. Lucas, C. F. R. Mackenzie, A. Mariko, T. Matulaitis, F. Millward, Y. Olivier, Q. Qi, I. D. W. Samuel, N. Sharma, C. Si, L. Spierling, P. Sudhakar, D. Sun, E. Tankelevičiūtė, M. Duarte Tonet, J. Wang, T. Wang, S. Wu, Y. Xu, L. Zhang and E. Zysman-Colman, The Golden Age of Thermally Activated Delayed Fluorescence Materials: Design and Exploitation, *Chem. Rev.*, 2024, **124**(24), 13736–14110, DOI: [10.1021/acs.chemrev.3c00755](https://doi.org/10.1021/acs.chemrev.3c00755).
- C. Adachi, M. A. Baldo, M. E. Thompson and S. R. Forrest, Nearly 100% Internal Phosphorescence Efficiency in an Organic Light-Emitting Device, *J. Appl. Phys.*, 2001, **90**(10), 5048–5051, DOI: [10.1063/1.1409582](https://doi.org/10.1063/1.1409582).
- Y. Tsuchiya, S. Diesing, F. Bencheikh, Y. Wada, P. L. Dos Santos, H. Kaji, E. Zysman-Colman, I. D. W. Samuel and C. Adachi, Exact Solution of Kinetic Analysis for Thermally Activated Delayed Fluorescence Materials, *J. Phys. Chem. A*, 2021, **125**(36), 8074–8089, DOI: [10.1021/acs.jpca.1c04056](https://doi.org/10.1021/acs.jpca.1c04056).
- N. Haase, A. Danos, C. Pflumm, A. Morherr, P. Stachelek, A. Mekic, W. Brütting and A. P. Monkman, Kinetic Modeling of Transient Photoluminescence from Thermally Activated Delayed Fluorescence, *J. Phys. Chem. C*, 2018, **122**(51), 29173–29179, DOI: [10.1021/acs.jpcc.8b11020](https://doi.org/10.1021/acs.jpcc.8b11020).
- T. J. Penfold, F. B. Dias and A. P. Monkman, The Theory of Thermally Activated Delayed Fluorescence for Organic Light Emitting Diodes, *Chem. Commun.*, 2018, **54**(32), 3926–3935, DOI: [10.1039/C7CC09612G](https://doi.org/10.1039/C7CC09612G).
- X.-K. Chen, D. Kim and J.-L. Brédas, Thermally Activated Delayed Fluorescence (TADF) Path toward Efficient Electroluminescence in Purely Organic Materials: Molecular Level Insight, *Acc. Chem. Res.*, 2018, **51**(9), 2215–2224, DOI: [10.1021/acs.accounts.8b00174](https://doi.org/10.1021/acs.accounts.8b00174).
- P. K. Samanta, D. Kim, V. Coropceanu and J.-L. Brédas, Up-Conversion Intersystem Crossing Rates in Organic Emitters for Thermally Activated Delayed Fluorescence: Impact of the Nature of Singlet vs Triplet Excited States, *J. Am. Chem. Soc.*, 2017, **139**(11), 4042–4051, DOI: [10.1021/jacs.6b12124](https://doi.org/10.1021/jacs.6b12124).
- K. Stavrou, L. G. Franca and A. P. Monkman, Photophysics of TADF Guest–Host Systems: Introducing the Idea of Hosting Potential, *ACS Appl. Electron. Mater.*, 2020, **2**(9), 2868–2881, DOI: [10.1021/acsaem.0c00514](https://doi.org/10.1021/acsaem.0c00514).
- H. Sun, C. Zhong and J.-L. Brédas, Reliable Prediction with Tuned Range-Separated Functionals of the Singlet–Triplet Gap in Organic Emitters for Thermally Activated Delayed Fluorescence, *J. Chem. Theory Comput.*, 2015, **11**(8), 3851–3858, DOI: [10.1021/acs.jctc.5b00431](https://doi.org/10.1021/acs.jctc.5b00431).
- I. A. Wright, A. Danos, S. Montanaro, A. S. Batsanov, A. P. Monkman and M. R. Bryce, Conformational Dependence of Triplet Energies in Rotationally Hindered N- and S-Heterocyclic Dimers: New Design and Measurement Rules for High Triplet Energy OLED Host Materials, *Chem. – Eur. J.*, 2021, **27**(21), 6545–6556, DOI: [10.1002/chem.202100036](https://doi.org/10.1002/chem.202100036).
- M. Y. Wong and E. Zysman-Colman, Purely Organic Thermally Activated Delayed Fluorescence Materials for Organic Light-Emitting Diodes, *Adv. Mater.*, 2017, **29**(22), 1605444, DOI: [10.1002/adma.201605444](https://doi.org/10.1002/adma.201605444).
- Y. Liu, C. Li, Z. Ren, S. Yan and M. R. Bryce, All-Organic Thermally Activated Delayed Fluorescence Materials for Organic Light-Emitting Diodes, *Nat. Rev. Mater.*, 2018, **3**(4), 18020, DOI: [10.1038/natrevmats.2018.20](https://doi.org/10.1038/natrevmats.2018.20).
- Y. Olivier, J.-C. Sancho-Garcia, L. Muccioli, G. D'Avino and D. Beljonne, Computational Design of Thermally Activated Delayed Fluorescence Materials: The Challenges Ahead, *J. Phys. Chem. Lett.*, 2018, **9**(20), 6149–6163, DOI: [10.1021/acs.jpcclett.8b02327](https://doi.org/10.1021/acs.jpcclett.8b02327).
- R. Walia, X. Xiong and X. C. Fan, *et al.*, Achieving small singlet–triplet energy gaps in polycyclic heteroaromatic emitters, *Nat. Mater.*, 2025, **24**, 1576–1583, DOI: [10.1038/s41563-025-02309-4](https://doi.org/10.1038/s41563-025-02309-4).
- Y. Tsuchiya, K. Mizukoshi and M. Saigo, *et al.*, Temperature dependency of energy shift of excitonic states in a donor–acceptor type TADF molecule, *Nat. Commun.*, 2025, **16**, 4815, DOI: [10.1038/s41467-025-59910-z](https://doi.org/10.1038/s41467-025-59910-z).
- N. Aizawa, Y. J. Pu and Y. Harabuchi, *et al.*, Delayed fluorescence from inverted singlet and triplet excited states, *Nature*, 2022, **609**, 502–506, DOI: [10.1038/s41586-022-05132-y](https://doi.org/10.1038/s41586-022-05132-y).



- 20 D. Kelly, L. G. Franca, K. Stavrou, A. Danos and A. P. Monkman, Laplace Transform Fitting as a Tool To Uncover Distributions of Reverse Intersystem Crossing Rates in TADF Systems, *J. Phys. Chem. Lett.*, 2022, **13**(30), 6981–6986, DOI: [10.1021/acs.jpcclett.2c01864](https://doi.org/10.1021/acs.jpcclett.2c01864).
- 21 J. Gibson, A. P. Monkman and T. J. Penfold, The Importance of Vibronic Coupling for Efficient Reverse Intersystem Crossing in Thermally Activated Delayed Fluorescence Molecules, *ChemPhysChem*, 2016, **17**(19), 2956–2961, DOI: [10.1002/cphc.201600662](https://doi.org/10.1002/cphc.201600662).
- 22 M. K. Etherington, J. Gibson, H. F. Higginbotham, T. J. Penfold and A. P. Monkman, Revealing the Spin–Vibronic Coupling Mechanism of Thermally Activated Delayed Fluorescence, *Nat. Commun.*, 2016, **7**(1), 13680, DOI: [10.1038/ncomms13680](https://doi.org/10.1038/ncomms13680).
- 23 X. Chen, Y. Tsuchiya, Y. Ishikawa, C. Zhong, C. Adachi and J. Brédas, A New Design Strategy for Efficient Thermally Activated Delayed Fluorescence Organic Emitters: From Twisted to Planar Structures, *Adv. Mater.*, 2017, **29**(46), 1702767, DOI: [10.1002/adma.201702767](https://doi.org/10.1002/adma.201702767).
- 24 P. De Silva, C. A. Kim, T. Zhu and T. Van Voorhis, Extracting Design Principles for Efficient Thermally Activated Delayed Fluorescence (TADF) from a Simple Four-State Model, *Chem. Mater.*, 2019, **31**(17), 6995–7006, DOI: [10.1021/acs.chemmater.9b01601](https://doi.org/10.1021/acs.chemmater.9b01601).
- 25 M. Moral, L. Muccioli, W.-J. Son, Y. Olivier and J. C. Sancho-García, Theoretical Rationalization of the Singlet–Triplet Gap in OLEDs Materials: Impact of Charge-Transfer Character, *J. Chem. Theory Comput.*, 2015, **11**(1), 168–177, DOI: [10.1021/ct500957s](https://doi.org/10.1021/ct500957s).
- 26 A. Pershin, D. Hall, V. Lemaire, J.-C. Sancho-García, L. Muccioli, E. Zysman-Colman, D. Beljonne and Y. Olivier, Highly Emissive Excitons with Reduced Exchange Energy in Thermally Activated Delayed Fluorescent Molecules, *Nat. Commun.*, 2019, **10**(1), 597, DOI: [10.1038/s41467-019-08495-5](https://doi.org/10.1038/s41467-019-08495-5).
- 27 S. Sem, S. Jenatsch, K. Stavrou, A. Danos, A. P. Monkman and B. Ruhstaller, Determining Non-Radiative Decay Rates in TADF Compounds Using Coupled Transient and Steady State Optical Data, *J. Mater. Chem. C*, 2022, **10**(12), 4878–4885, DOI: [10.1039/D1TC05594A](https://doi.org/10.1039/D1TC05594A).
- 28 L. Salah, M. K. Etherington, A. Shuaib, A. Danos, A. A. Nazeer, B. Ghazal, A. Prlj, A. T. Turley, A. Mallick, P. R. McGonigal, B. F. E. Curchod, A. P. Monkman and S. Makhseed, Suppressing Dimer Formation by Increasing Conformational Freedom in Multi-Carbazole Thermally Activated Delayed Fluorescence Emitters, *J. Mater. Chem. C*, 2021, **9**(1), 189–198, DOI: [10.1039/D0TC04222F](https://doi.org/10.1039/D0TC04222F).
- 29 D. Chen, L. Zhang, T. Matulaitis, D. B. Cordes, A. M. Z. Slawin, X.-H. Zhang, I. D. W. Samuel and E. Zysman-Colman, Tuning the Emission and Exciton Utilization Mechanisms of Pyrazine-Based Multi-Carbazole Emitters and Their Use in Organic Light-Emitting Diodes, *J. Mater. Chem. C*, 2023, **11**(38), 13095–13105, DOI: [10.1039/D3TC02463F](https://doi.org/10.1039/D3TC02463F).
- 30 D. Chen, J. Gong, J. Grüne, T. Matulaitis, A. J. Gillett, X. Zhang, I. D. W. Samuel, G. A. Turnbull and E. Zysman-Colman, Tetra-Donor Pyrazine Based Thermally Activated Delayed Fluorescence Emitters for Electroluminescence and Amplified Spontaneous Emission, *Adv. Funct. Mater.*, 2024, **34**(49), 2409592, DOI: [10.1002/adfm.202409592](https://doi.org/10.1002/adfm.202409592).
- 31 R. Crespo-Otero and M. Barbatti, Spectrum Simulation and Decomposition with Nuclear Ensemble: Formal Derivation and Application to Benzene, Furan and 2-phenylfuran, *Theor. Chem. Acc.*, 2012, **131**, 1237, DOI: [10.1007/s00214-012-1237-4](https://doi.org/10.1007/s00214-012-1237-4).
- 32 A. Prlj, E. Marsili, L. Hutton, D. Hollas, D. Shepchanovska, D. R. Glowacki, P. Slavíček and B. F. E. Curchod, Calculating Photoabsorption Cross-Sections for Atmospheric Volatile Organic Compounds, *ACS Earth Space Chem.*, 2022, **6**, 207–217, DOI: [10.1021/acsearthspacechem.1c00355](https://doi.org/10.1021/acsearthspacechem.1c00355).
- 33 L. E. de Sousa and P. de Silva, Unified framework for photo-physical rate calculations in TADF molecules, *J. Chem. Theory Comput.*, 2021, **17**, 5816–5824, DOI: [10.1021/acs.jctc.1c00476](https://doi.org/10.1021/acs.jctc.1c00476).
- 34 A. J. Gillett, A. Pershin and R. Pandya, *et al.*, Dielectric control of reverse intersystem crossing in thermally activated delayed fluorescence emitters, *Nat. Mater.*, 2022, **21**, 1150–1157, DOI: [10.1038/s41563-022-01321-2](https://doi.org/10.1038/s41563-022-01321-2).
- 35 R. Huang, N. A. Kukhta, J. S. Ward, A. Danos, A. S. Batsanov, M. R. Bryce and F. B. Dias, Balancing Charge-Transfer Strength and Triplet States for Deep-Blue Thermally Activated Delayed Fluorescence with an Unconventional Electron Rich Dibenzothiophene Acceptor, *J. Mater. Chem. C*, 2019, **7**(42), 13224–13234, DOI: [10.1039/c9tc02175b](https://doi.org/10.1039/c9tc02175b).
- 36 P. Imbrasas, R. Lygaitis, P. Kleine, R. Scholz, C. Hänisch, S. Buchholtz, K. Ortstein, F. Talnack, S. C. B. Mannsfeld, S. Lenk and S. Reineke, Dimers or Solid-State Solvation? Intermolecular Effects of Multiple Donor–Acceptor Thermally Activated Delayed Fluorescence Emitter Determining Organic Light-Emitting Diode Performance, *Adv. Opt. Mater.*, 2021, **9**(14), 2002153, DOI: [10.1002/adom.202002153](https://doi.org/10.1002/adom.202002153).
- 37 T. Serevičius, R. Skaisgiris, D. Gudeika, K. Kazlauskas and S. Juršėnas, Conformational Disorder Enabled Emission Phenomena in Heavily Doped TADF Films, *Phys. Chem. Chem. Phys.*, 2022, **24**(1), 313–320, DOI: [10.1039/d1cp04905d](https://doi.org/10.1039/d1cp04905d).
- 38 M. K. Etherington, N. A. Kukhta, H. F. Higginbotham, A. Danos, A. N. Bismillah, D. R. Graves, P. R. McGonigal, N. Haase, A. Morherr, A. S. Batsanov, C. Pflumm, V. Bhalla, M. R. Bryce and A. P. Monkman, Persistent Dimer Emission in Thermally Activated Delayed Fluorescence Materials, *J. Phys. Chem. C*, 2019, **123**(17), 11109–11117, DOI: [10.1021/acs.jpcc.9b01458](https://doi.org/10.1021/acs.jpcc.9b01458).
- 39 M. Hempe, N. A. Kukhta, A. Danos, A. S. Batsanov, A. P. Monkman and M. R. Bryce, Intramolecular Hydrogen Bonding in Thermally Activated Delayed Fluorescence Emitters: Is There Evidence Beyond Reasonable Doubt, *J. Phys. Chem. Lett.*, 2022, **13**(35), 8221–8227, DOI: [10.1021/acs.jpcclett.2c00907](https://doi.org/10.1021/acs.jpcclett.2c00907).
- 40 M. Hempe, N. A. Kukhta, A. Danos, M. A. Fox, A. S. Batsanov, A. P. Monkman and M. R. Bryce, Vibrational Damping Reveals Vibronic Coupling in Thermally Activated Delayed Fluorescence Materials, *Chem. Mater.*, 2021, **33**(9), 3066–3080, DOI: [10.1021/acs.chemmater.0c03783](https://doi.org/10.1021/acs.chemmater.0c03783).

